Nanoscale

PAPER

View Article Online
View Journal | View Issue

Cite this: *Nanoscale*, 2016, **8**, 11114

Coaxial carbon@boron nitride nanotube arrays with enhanced thermal stability and compressive mechanical properties†

Lin Jing,[a,b] Roland Yingjie Tay,[c,d] Hongling Li,[c,e] Siu Hon Tsang,[d] Jingfeng Huang,[a,b] Dunlin Tan,[c,e] Bowei Zhang,[a] Edwin Hang Tong Teo*[a,c] and Alfred Iing Yoong Tok*[a,b]

Received 11th February 2016,
Accepted 27th April 2016

DOI: 10.1039/c6nr01199c

www.rsc.org/nanoscale

Vertically aligned carbon nanotube (CNT) arrays have aroused considerable interest because of their remarkable mechanical properties. However, the mechanical behaviour of as-synthesized CNT arrays could vary drastically at a macro-scale depending on their morphologies, dimensions and array density, which are determined by the synthesis method. Here, we demonstrate a coaxial carbon@boron nitride nanotube (C@BNNT) array with enhanced compressive strength and shape recoverability. CNT arrays are grown using a commercially available thermal chemical vapor deposition (TCVD) technique and an outer BNNT with a wall thickness up to 1.37 nm is introduced by a post-growth TCVD treatment. Importantly, compared to the as-grown CNT arrays which deform almost plastically upon compression, the coaxial C@BNNT arrays exhibit an impressive ~4-fold increase in compressive strength with nearly full recovery after the first compression cycle at a 50% strain (76% recovery maintained after 10 cycles), as well as a significantly high and persistent energy dissipation ratio (~60% at a 50% strain after 100 cycles), attributed to the synergistic effect between the CNT and outer BNNT. Additionally, the as-prepared C@BNNT arrays show an improved structural stability in air at elevated temperatures, attributing to the outstanding thermal stability of the outer BNNT. This work provides new insights into tailoring the mechanical and thermal behaviours of arbitrary CNT arrays which enables a broader range of applications.

Introduction

Vertically aligned carbon nanotube (CNT) arrays have been recognized as promising multifunctional and high performance structural materials due to their exceptional electrical,[1] thermal[2] and in particular their mechanical properties.[3–6] Despite their low density, CNT arrays normally exhibit high mechanical strength and stiffness.[7,8] In addition, CNT arrays also possess a unique buckling response upon uniaxial compression[7,9] that allows for energy dissipation through structural deformation and friction between the individual CNTs. Owing to these interesting characteristics, CNT arrays have been applied in a wide range of applications, including compliant thermal interface with low inter-facial resistance,[10] nano/micro-electromechanical systems (NEMS/MEMS),[11] as well as efficient energy dissipating systems for shockwave,[12,13] acoustic[14] and vibration absorptions.[15–18] Moreover, CNT arrays have also been used as fillers for toughening of materials.[19,20] However, it is worth noting that their mechanical properties strictly depend on the geometrical structure of the CNTs and their buckling behaviour is closely associated with the interactions between individual tubes.[16,17,21–23] Thus far, the most common method to synthesize CNT arrays has been thermal chemical vapour deposition (TCVD), while this growth process usually produces CNTs with thin walls, low packing density and weak inter-tube interactions, which lead to their plastic deformation upon compression.[16,21,24–26] Furthermore, CNTs are known to oxidize readily at ~400 °C when exposed to air,[27–29] which restricts their post-process treatment and applications in a high temperature environment. To address the abovementioned issues, many efforts have been made either by modifying their microstructure through alter-

[a]*School of Materials Science and Engineering, Nanyang Technological University, 50 Nanyang Avenue, Singapore 639798, Singapore. E-mail: MIYTOK@ntu.edu.sg*
[b]*Institute for Sports Research, Nanyang Technological University, 50 Nanyang Avenue, Singapore 639798, Singapore*
[c]*School of Electrical and Electronic Engineering, Nanyang Technological University, 50 Nanyang Avenue, Singapore 639798, Singapore. E-mail: HTTEO@ntu.edu.sg*
[d]*Temasek Laboratories@NTU, 50 Nanyang Avenue, Singapore 639798, Singapore*
[e]*CNRS-International NTU Thales Research Alliance CINTRA UMI 3288, Research Techno Plaza, 50 Nanyang Drive, Singapore 637553, Singapore*

†Electronic supplementary information (ESI) available: Additional compressive stress–strain curves for as-grown CNT and C@BNNT$_{40}$ arrays at various applied strains. SEM images of as-grown CNT and C@BNNT$_{60}$ arrays before and after annealing. SEM and representative TEM images of C@BNNT before and after cyclic compression. See DOI: 10.1039/c6nr01199c

ing the growth process[23,26,30] or applying post-growth treatment to reinforce the as-grown CNT arrays.[16,20,31–33] Particularly, the latter approach which involves the thickening of the tube diameter and increase in the array density of the CNT arrays has been widely studied to strengthen arbitrary CNT arrays. Recent examples include coating metal oxide nanoparticles onto CNTs,[32,33] infiltrating a polymer into the interspaces of CNTs[20] and introducing other forms of carbon (additional CNT walls or graphene sheets) into arrays.[16,31]

On the other hand, as a structural analogue of CNT,[34–36] a boron nitride nanotube (BNNT) has also been proved to possess superior mechanical properties[37–39] and excellent oxidation resistance at relatively high temperatures (~700 to 900 °C).[27] However, the mechanical-related applications for as-grown BNNTs are not yet mature due to the challenges in synthesizing densely packed and high quality BNNT arrays with suitable dimensions.[40–46] Still, due to its outstanding physicochemical stability, a BNNT has been applied as a protective coating material for a CNT.[47,48] Few have already reported the synthesis of BN coated CNTs for field emission applications with improved lifetime and stability.[49–51] Recently, BN coated single-walled CNT aerogels have been prepared by a solution based assembly process and exhibited enhanced elastic modulus and shape recoverability.[52] Furthermore, it has also been predicted theoretically that not only the high thermal resistance of the outer BNNT can provide protection for the inner CNT, but also the inter-wall van der Waals interactions between the CNT and BNNT will further enhance the protective effect of the outer BNNT both thermally and mechanically.[53,54] However, to the best of our knowledge, such reinforcements have not been investigated experimentally.

Herein, we report the fabrication of coaxial BNNT encapsulated CNT (C@BNNT) arrays with two different BN weight ratios *via* a two-step growth TCVD method by firstly, the growth of the CNT arrays and subsequently, encapsulation of the CNTs with BNNTs. Uniaxial compression tests were carried out before and after air annealing to characterize the effects of the outer BNNTs with different wall thicknesses on the mechanical and thermal performances of the C@BNNT arrays. The changes in the morphology and areal density of the NTs before and after encapsulation/compression/annealing were analysed by performing scanning electron microscopy (SEM) investigations. Importantly, the compressive mechanical properties of the C@BNNT arrays could be tailored by varying the wall thickness of the outer BNNT. Furthermore, the compressive strength, shape recoverability, cyclic compressive and energy dissipating properties, as well as structural stability in air at elevated temperatures have been significantly enhanced due to the synergistic effect between the CNT and the outer BNNT.

Experimental section

Preparation of vertically aligned CNT arrays

CNT arrays were grown using TCVD on a Si substrate with a sandwich-structured catalyst layer consisting of 6 nm Al, 4 nm Al_2O_3 and 1 nm Fe and fabricated by electron beam deposition. The CNT was grown at a pressure of 720 mbar with flowing gases including H_2 (200 sccm, using as an etching gas), N_2 (160 sccm, using as a carrier gas) and C_2H_2 (15 sccm, using as a carbon source). The Si substrate was heated up to 730 °C and maintained for 20 min to sustain the growth of CNT arrays with an average height of ~0.4 mm.

Fabrication of C@BNNT arrays

C@BNNT arrays were prepared by TCVD according to a previously reported method with slight modification.[55] Briefly, the CNT samples on the Si wafer were firstly located in the central part of a horizontal reaction tube and boric acid powder with a specified amount was loaded at one end of the tube, followed by heating up to 150 °C for 10 min and holding for 30 min under flowing Ar (300 sccm). The temperature was then ramped up to 830 °C in 90 min and retained for another 30 min. Ammonia with a desired flow rate was introduced into the tube when boric acid started to sublimate, and the flow rate of Ar was adjusted accordingly to keep the total flow rate of gases in the tube constant. Finally, the tube was further heated up to 900 °C and maintained for another 1 h, followed by naturally cooling down to room temperature under protection of an Ar flow. For simplicity, C@BNNTs with BN weight ratios of ~40% and 60% were designated as $C@BNNT_{40}$ and $C@BNNT_{60}$, respectively. By sintering the as-prepared samples at 400 °C for 1 h in air, annealed CNT and $C@BNNT_{60}$ arrays were also successfully prepared, respectively.

Mechanical test

The mechanical responses of the CNT and C@BNNT arrays before and after annealing were measured using an Instron 5567 Mechanical Tester system at room temperature. In general, the CNT or C@BNNT sample with a specified dimension was firstly loaded at the centre of the lower platen, a compression rod with 50 mm diameter was then applied onto the sample with a controlled speed, and all the compressions were conducted within the confinement of the small upper platen. Compressive strain and stress were calculated using the displacement of the compression rod divided by the original height of the NT arrays and the applied compressive force over the cross-sectional area of the samples, respectively. Recoverability of the NT arrays is defined as the displacement recovered over applied displacement. For the CNT, $C@BNNT_{40}$ and $C@BNNT_{60}$ arrays, the cyclic uniaxial compression experimental data were acquired at a loading–unloading rate of 0.04 mm min^{-1} at strains of 30%, 50%, 70%, and 90%, respectively. For the annealed CNT and $C@BNNT_{60}$ arrays, the data were collected at strains of 50% and 90%, respectively, while keeping all other test parameters unchanged.

Characterization

Field emission scanning electron microscopy (FESEM, JEOL JSM-7600F) was performed to characterize the change in the morphology and areal density of the NTs before and after encapsulation/uniaxial compression/annealing. Nano-

structures of the as-prepared CNT and C@BNNT were characterized by high resolution transmission electron microscopy (TEM, JEOL JEM-2100F). The thermal behaviours of the CNT and C@BNNT samples were analysed by thermogravimetric analysis (TGA, Shimadzu DTG-60H thermal analyser) under a constant flow of air (50 ml min^{-1}) and heated from 30 to 1100 °C at a heating rate of 10 °C min^{-1}. Fourier transform infrared spectroscopy (FT-IR, IRPrestige-21 spectrometer) was performed within wavenumbers ranging from 4000 to 400 cm^{-1}. Raman spectroscopy (WITEC CRM200 Raman system) was performed to study the crystal structures of the NT arrays using a laser of 532 nm wavelength.

Results and discussion

In this work, CNT arrays were grown by a commercialized TCVD process on Si substrates with defined catalyst areas and C@BNNT arrays were prepared with the aid of another separate TCVD process as described in our previous report.[55] By varying the growth parameters, two sets of C@BNNT arrays with specified BNNT wall thicknesses denoted as $C@BNNT_{40}$ and $C@BNNT_{60}$ were successfully fabricated (see the Experimental section). Fig. 1a–c show the cross-sectional SEM images of the CNT and C@BNNT arrays, respectively. It is obvious that the C@BNNT arrays retained the vertically aligned structure of the initial CNT arrays with no observable change in the areal density. To investigate the wall thickness of the outer BNNT, a systematic TEM study on various NTs was further carried out. Fig. 1d–f show representative high resolution TEM images of the individual CNT, $C@BNNT_{40}$ and $C@BNNT_{60}$, respectively. The initial CNT exhibited an inner diameter of 6.25 nm with an average wall thickness of 1.15 nm (corresponding to 3 to 4 walls). An increase in the wall thickness was observed for both $C@BNNT_{40}$ and $C@BNNT_{60}$ which was measured to be 1.60 and 2.52 nm, respectively. Based on

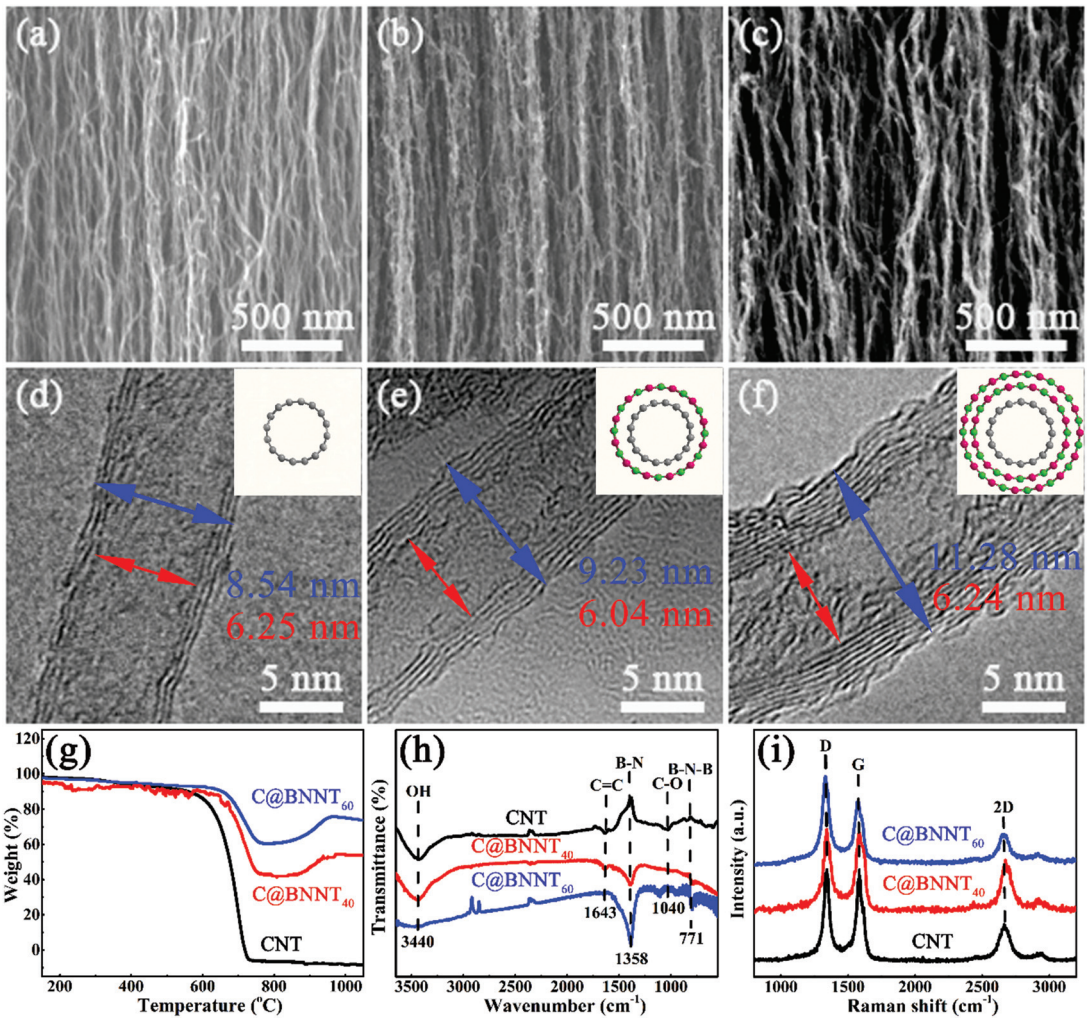

Fig. 1 Cross-sectional SEM and corresponding high resolution TEM images of (a, d) CNT, (b, e) $C@BNNT_{40}$ and (c, f) $C@BNNT_{60}$, respectively. BNNTs with increasing wall thicknesses were successfully encapsulated onto the CNTs without causing any observable change in the areal density of the NTs. TGA (g), FT-IR (h), and Raman (i) spectra of the various NTs, indicating that the crystal structure of the CNTs was preserved after the introduction of outer BNNTs with different weight ratios.

the TEM images, outer BNNTs with wall thicknesses of 0.45 nm (~2 walls) and 1.37 nm (~5 walls) were introduced into C@BNNT$_{40}$ and C@BNNT$_{60}$, respectively. Thus, the C@BNNT arrays with outer BNNTs of varying wall thicknesses can be achieved by altering the experimental parameters.

To further determine the BN contents of the C@BNNT arrays, thermogravimetric analysis (TGA) was employed and the weight residues at temperatures lower than 700 °C were extracted. TGA tests were conducted in air from 30 to 1100 °C, as shown in Fig. 1g. It is observed that the CNTs fully decomposed at 700 °C while 41.3% and 60.3% weight residues emerged for the C@BNNT samples, indicating that the weight ratios of BN : C were ~40 : 60 and 60 : 40 for C@BNNT$_{40}$ and C@BNNT$_{60}$, respectively, which were in good agreement with our TEM results. It should be noted that the increase in weight at ~900 °C for C@BNNT is due to the partial oxidation of BNNT forming B_2O_3.[55] Fig. 1h and i present the FT-IR and Raman spectra of the CNT, C@BNNT$_{40}$ and C@BNNT$_{60}$, respectively. In Fig. 1h, a characteristic C=C stretching at 1643 cm^{-1} is observed for CNT, while additional B–N–B and B–N vibrations located at 771 and 1358 cm^{-1} can be clearly seen for C@BNNT, respectively.[56] Raman spectra of all the NTs show the characteristic D, G and 2D peaks at ~1350, 1580 and 2700 cm^{-1}, respectively (Fig. 1i), implying that the crystal structure of the CNT was preserved after encapsulating with BNNT.[49,55]

Uniaxial compression tests of the CNT and C@BNNT arrays were carried out to study their mechanical behaviours. Fig. 2 schematically illustrates the compression behaviours of the CNT arrays before and after encapsulating with BNNT. Both CNT and C@BNNT arrays were compressed uniaxially along the longitudinal direction (nanotube axis) at a certain strain. As-grown CNT arrays deformed almost plastically upon compression, while the introduced outer BNNT enabled the C@BNNT arrays to become resilient and exhibit shape recovery upon the release of the compressive load.

Fig. 3a shows the compressive stress *vs.* strain loading-unloading curves for the CNT, C@BNNT$_{40}$ and C@BNNT$_{60}$ arrays. The as-grown CNT arrays that were compressed at a 90% strain recovered only ~6% upon load releasing and showed analogous responses also at strains ranging from 10% to 80% (Fig. S1†). A similar phenomenon has also been observed in previously reported work, attributed to the small tube diameter (~8 nm) and thin wall thickness (1.15 nm, ~3 walls), which were determined by a specific fabrication setup and synthesis method.[6,16,21,23–26] When the BN weight ratio of C@BNNT arrays increased to 40%, a partial recovery (~33%) upon unloading emerged, while ~77% recovery was observed for the C@BNNT$_{60}$ arrays after unloading of 90% compressive strain, and the two distinct paths corresponding to loading and unloading processes respectively compose a hysteresis loop. In addition, the C@BNNT arrays showed an impressive ~4-fold increase in the compressive strength (from 0.47 to 2.47 MPa) with an enhanced compressive modulus, and exhibited nonlinear behaviour as observed by the increase in the compressive modulus with increasing the applied strain. The recoverability of the C@BNNT arrays was further investigated at various applied strains of 30%, 50%, 70% and 90%, respectively, as shown in Fig. 3b and c. It is observed that the C@BNNT$_{40}$ and C@BNNT$_{60}$ arrays exhibited similar strain-dependent mechanical responses under compressions where the peak compressive stress increased with increasing applied strains, while showing differences in their recovery processes. For the C@BNNT$_{40}$ arrays, a partial recovery of ~40% was observed after compressions at various applied strains while with no critical strain value for full recovery (Fig. 3b and S2†). In contrast, the C@BNNT$_{60}$ arrays exhibited almost a full shape recovery when a compressive strain of 50% or less was applied and partial recoveries of ~79% and 77% were observed when the applied strain was increased to 70% and 90%, respectively (Fig. 3c).

Considering the high porosity, resilience and compressive strength of the C@BNNT arrays, they are expected to show promising energy absorbing abilities.[7] To quantitatively characterize the energy dissipating properties of the NT arrays, their energy dissipation ratios, E_d/E_a, are extracted from their corresponding stress *vs.* strain curves, where E_d is the energy dissipated during the loading–unloading cycle (*i.e.* the area of the hysteresis loop), and E_a is the energy absorbed from compression loading (*i.e.* the area under the loading stress–strain curve).[57] As shown in Fig. 3d, both the C@BNNT$_{40}$ and C@BNNT$_{60}$ arrays showed a strain-dependent energy dissipating performance. The C@BNNT$_{40}$ arrays exhibited E_d/E_a of 75.27%, 79.72%, 85.53%, and 86.25% at applied strains of 30%, 50%, 70% and 90%, respectively, while the C@BNNT$_{60}$ arrays with better shape recoverability exhibited relatively lower E_d/E_a of 57.33%, 71.45%, 74.86% and 78.36% at respective strains, attributed to the smaller permanent shape deformation and larger energy return. By comprehensively considering the abovementioned aspects, it is expected that the C@BNNT$_{60}$ arrays are more suitable for applications where both energy absorption and load recovery are critical.

To gain insights into the compression mechanisms of the NT arrays, cross-sectional SEM images were taken on the CNT, C@BNNT$_{40}$ and C@BNNT$_{60}$ arrays before and after cyclic compressions (Fig. 4). Fig. 4a, d and b, e show the CNT and C@BNNT$_{40}$ arrays before and after 3 compression cycles at a

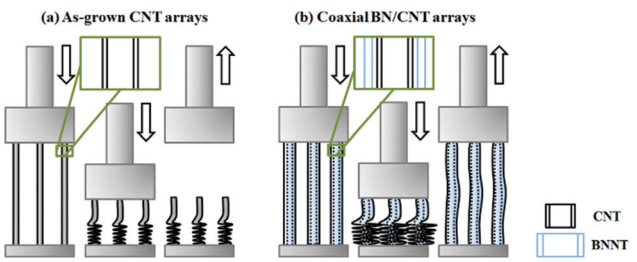

Fig. 2 Schematic illustrations of the compressive behaviours of the (a) CNT and (b) C@BNNT arrays. The as-grown CNT arrays underwent plastic deformation upon compression, while the additional outer BNNT walls facilitated the elastic recovery of the C@BNNT arrays after load releasing.

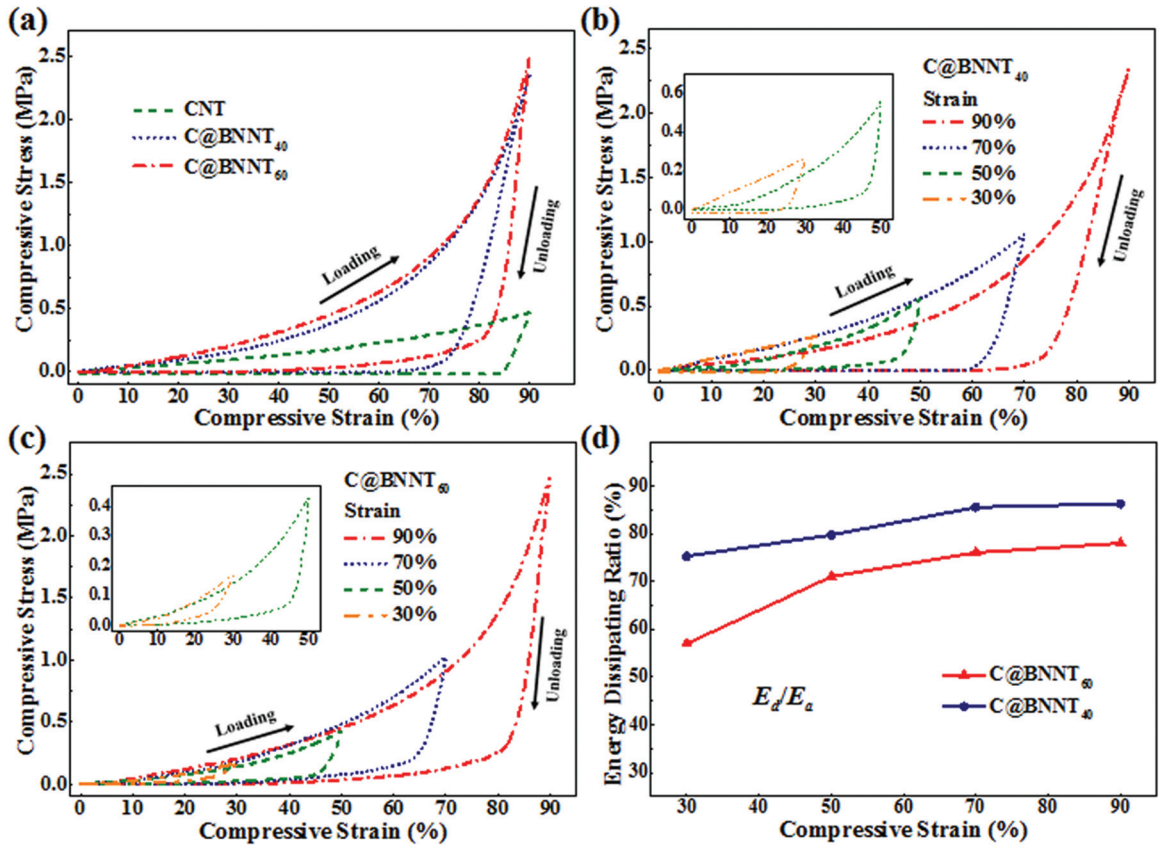

Fig. 3 Compressive stress *vs.* strain curves for the (a) CNT, C@BNNT$_{40}$ and C@BNNT$_{60}$ arrays at a 90% strain, (b, c) C@BNNT$_{40}$ and C@BNNT$_{60}$ arrays at strains of 30%, 50%, 70% and 90%, and (d) the energy dissipation ratio of the C@BNNT arrays *vs.* the applied strain. The C@BNNT arrays exhibited controllably enhanced compressive strength, modulus, and shape recoverability compared to the as-grown CNT arrays.

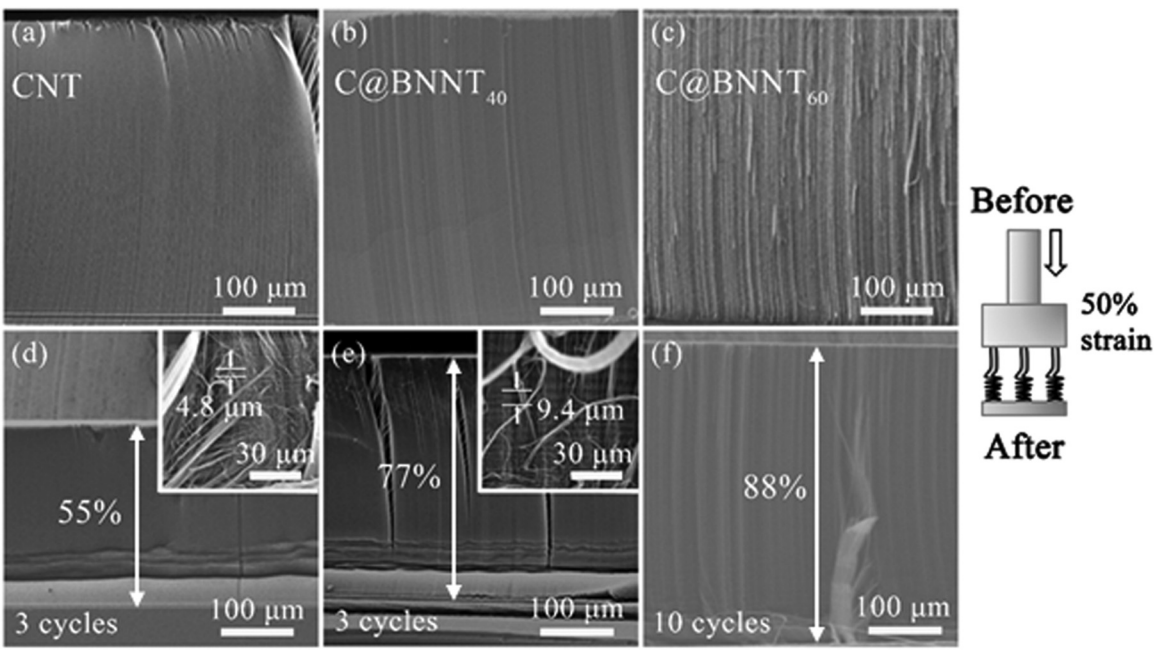

Fig. 4 Cross-sectional SEM images of the NT arrays after cyclic compressions. The CNT arrays (a, d) deformed almost plastically with heavy buckles (inset) at the bottom region, while the C@BNNT$_{40}$ arrays (b, e) and the C@BNNT$_{60}$ arrays (c, f) exhibited partial recovery with slight buckles (inset) and nearly full recovery with only curvatures formed on the tubes, respectively, showing the significantly promoted compressive resilience of the C@BNNT arrays.

50% strain, respectively. It is observed that the CNT arrays collapsed with minute recovery (55% of the original height was maintained) and local buckling initiated from the bottom of the CNTs which propagated upwards with a constant buckle wavelength of ~4.8 μm (Fig. 4a and d). This local buckling can be attributed to the relatively lower areal density and smaller diameter of the CNTs at the bottom region (Fig. S3c and e†) as they follow a "bottom-up growth" mechanism (*i.e.* the CNTs grow upwards from the bottom catalyst side).[21,23,58] Furthermore, unbalanced friction between the substrate and the bottom NTs could also have some contributions as well.[22] In contrast, ~54% recovery was displayed (77% of the original height remained) for the C@BNNT$_{40}$ arrays and buckles with a longer average wavelength of ~9.4 μm could be observed at the bottom of the NTs (Fig. 4b and e). The evident increase in the buckle wavelength of the compressed C@BNNT$_{40}$ arrays indicates that they possess higher compressive resilience compared to the starting CNT arrays.[59] Hence, the outer BNNT played a significant role in enhancing the overall compressive resilience of the NT arrays. As an additional outer BNNT was encapsulated onto the CNT, radial thickening was evident which provided additional mechanical support to the NTs.[16,23] More importantly, the stable van der Waals interactions between the BNNT wall and the adjacent CNT wall upon compression protected the inner CNT from buckling, thus improving the effective compressive resistance and stiffness of the NT arrays.[53]

Fig. 4c and f show the SEM images of the C@BNNT$_{60}$ arrays before and after 10 compression cycles at a 50% stain. It is noted that the C@BNNT$_{60}$ arrays exhibited an ~76% recovery (maintaining 88% of the original height) even after 10 compression cycles, while only longitudinal distributed curvatures (*i.e.* buckles with ultra-long wavelengths) were observed, indicating significant enhancement in the compressive resilience, which further increase the wall thickness of outer BNNT. It is noted that the curvature length was gradually decreased from upper to bottom portions (Fig. 4f), and a similar gradient in the buckle wavelength was also observed on compressed C@BNNT$_{40}$ arrays (Fig. 4e), demonstrating the densification behaviour of the C@BNNT arrays under compression.[7,22] This can be attributed to the strengthened lateral interactions (*i.e.* van der Waals interactions) between the NTs due to the smaller inter-tube spacing after the introduction of the outer BNNT, resulting in the nonlinear stress–strain relationship of the C@BNNT arrays.[8,22] However, no additional interfacial frictions were induced between the NTs for C@BNNT arrays due to the exceptionally lower friction between the BNNTs than that between the CNTs.[60,61] Moreover, the contact area between the adjacent NTs became larger with a further increased wall thickness of the outer BNNT, longitudinal sliding was hence decoupled due to the transversal deformation, resulting in lower longitudinal shear strength.[61] Therefore, no apparent improvement in compressive strength was observed on the C@BNNT$_{60}$ arrays compared to the C@BNNT$_{40}$ arrays (Fig. 3a).

In addition, it is noted that the C@BNNT$_{60}$ arrays can endure the impact of thermal treatment and preserve their excellent compressive mechanical performance. Both the C@BNNT$_{60}$ and CNT arrays were annealed in air at 400 °C for 1 h, respectively, prior to compression tests. As shown in Fig. 5a and b, the annealed CNT arrays exhibited an overall substantial decrease in the compressive strength and modulus at both 90% and 50% applied strains, and additional deformations (white arrows in Fig. 5c) were found at the top portion of the annealed CNT arrays after compression, attributed to the oxidation induced defects[27] and decreased areal density of NTs (Fig. S3†). While the annealed C@BNNT$_{60}$ arrays were able to perfectly retain their mechanical response and structure (Fig. 5d) at a 50% strain, a decrease of the stress response was only observed at larger applied strains, resulting from the partial oxidation of the top portion of the inner CNTs due to improved access to air molecules (Fig. S4†).[62] Therefore, thermally stable C@BNNT$_{60}$ arrays with excellent compression behaviour facilitated by the protection of outer BNNTs show great potential in high temperature applications.

To study the long-term cyclic mechanical performance of the C@BNNT and CNT arrays, uniaxial cyclic compression was further applied at a 50% strain. As shown in Fig. 6a, the CNT arrays underwent serious plastic deformation during their first loading–unloading compression cycle followed by minute

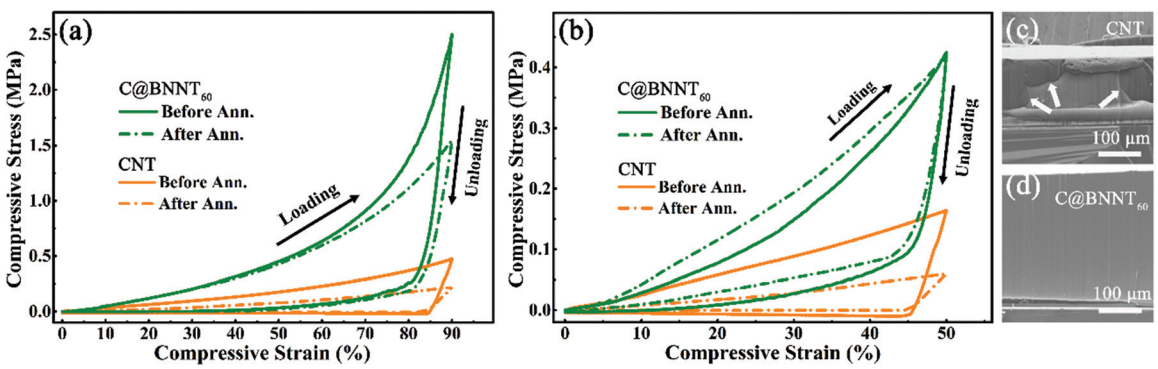

Fig. 5 Compressive stress *vs.* strain curves for the CNT and C@BNNT$_{60}$ arrays before and after annealing (ann.) at strains of (a) 90% and (b) 50%, respectively. Cross-sectional SEM images of the annealed CNT (c) and C@BNNT$_{60}$ (d) arrays after 3 cycles at a 50% strain. White arrows in (c) show the additional deformations of the annealed CNT arrays. The outer BNNTs protected most of the CNTs from oxidation-induced degradation.

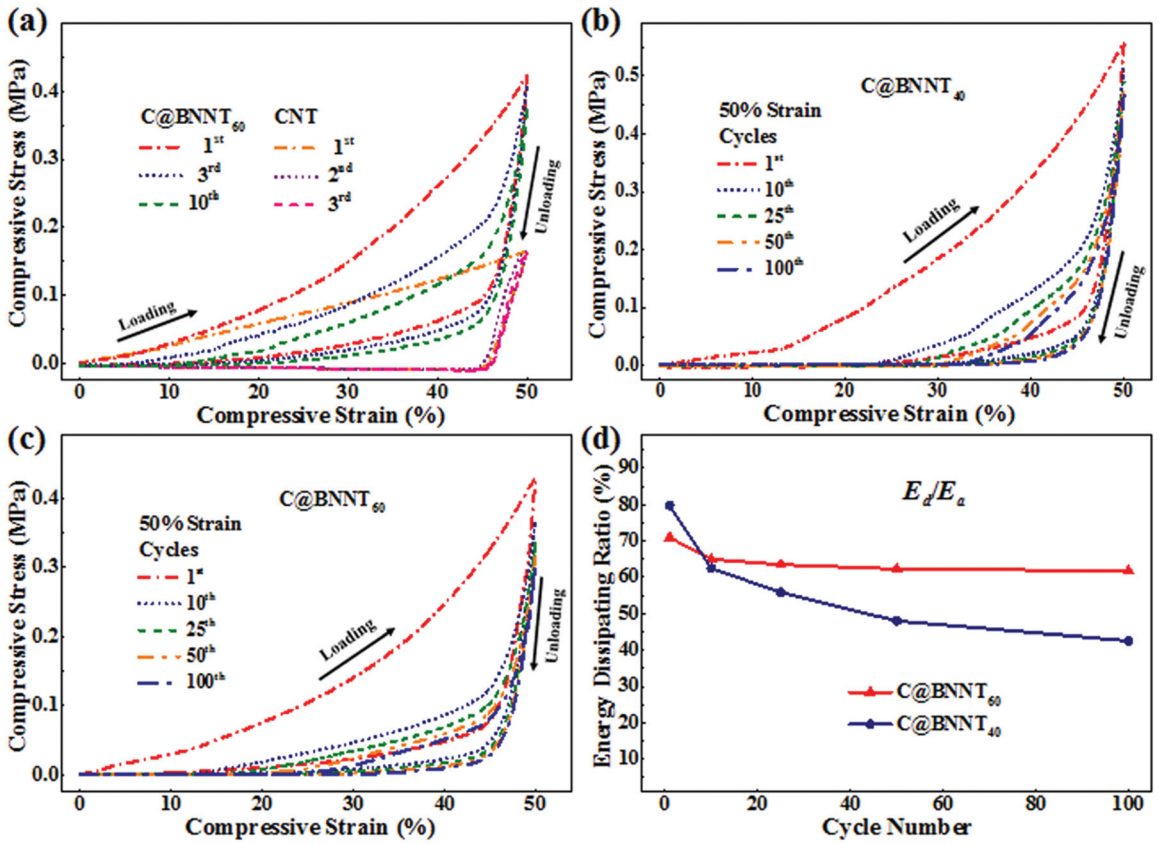

Fig. 6 Cyclic compressive stress *vs.* strain curves at a 50% strain for (a) comparison of the C@BNNT$_{60}$ and CNT arrays; (b, c) C@BNNT$_{40}$ and C@BNNT$_{60}$ arrays under 100 cycles of compression, respectively, and (d) the energy dissipation ratio of the C@BNNT arrays as a function of cycle number. The C@BNNT arrays exhibited significantly enhanced cyclic compressive mechanical properties, and the preconditioning effect was observed.

elastic recovery during the subsequent cycles as a result of the reversible compressions of the compressed portion,[23] while the C@BNNT$_{60}$ arrays displayed almost 100% recovery after the first compression cycle with slight degradation of recoverability in the subsequent cycles (~76% remained after 10 cycles). For the as-grown CNT arrays, the unfolding or unpacking of the bent CNTs after the release of the load was hindered by the strong van der Waals attraction between the compressed CNTs, while for the C@BNNT$_{60}$ arrays, the stronger generated restoring force upon load releasing over the van der Waals interactions among the NTs led to their significantly improved recoverability.[16,23] Fig. 6b and c show the representative stress–strain curves of the C@BNNT$_{40}$ and C@BNNT$_{60}$ arrays under 100 cycles of compression, respectively. A transient phenomenon in compressive strength (preconditioning effect) can be observed for the C@BNNT arrays. The compressive strength of the C@BNNT$_{40}$ arrays was measured to be up to ~0.55 MPa during the initial cycles, which gradually decreased to ~0.49 MPa and kept almost unchanged after 50 cycles. A similar strength evolution was also observed for the C@BNNT$_{60}$ arrays (from ~0.42 to ~0.35 MPa). This stress softening was due to the weakened van der Waals inter-tube interactions and the compression induced defects during the initial several cycles,[18,63,64] after which a new equilibrium status (collectively buckled, as shown in Fig. S5†) was gradually reached to achieve a stable stress response. In addition, the shape recoverability of the C@BNNT arrays evolved gradually with increasing cycles (~68% and 78% of their original height remained for the C@BNNT$_{40}$ and C@BNNT$_{60}$ arrays after 100 cycles, respectively), as identified by the corresponding SEM images (Fig. S5†). This persistent shape recovery performance was facilitated by the effective protection of the outer BNNT walls, as no changes in the structural dimensions of the C@BNNT were observed throughout the long-term compressive tests (Fig. S6†). Furthermore, a greater decline in the E_d/E_a of the C@BNNT$_{40}$ arrays (from 79.72% to 45.23%) with the increasing cycles was observed compared to that of the C@BNNT$_{60}$ (from 71.35% to 61.81%), which remained somewhat consistent after 100 cycles (Fig. 6d), indicating that the enhanced shape recoverability will enable a more stable energy dissipating performance over long-term cycling.

Conclusion

CNT and coaxial BNNT encapsulated CNT (C@BNNT) arrays with two different BN weight ratios (C@BNNT$_{40}$ and C@BNNT$_{60}$) were successfully prepared and their mechanical

behaviours were systematically investigated using uniaxial compression tests at various applied strains and compression cycles. Importantly, the compressive mechanical properties of the C@BNNT arrays can be controllably tuned by varying the wall thickness of the outer BNNT. A tremendous ~4-fold increase in the compressive strength of the C@BNNT arrays was achieved by reinforcing the CNT arrays with outer BNNTs. Furthermore, as compared to the as-grown CNT arrays which almost plastically deformed upon compression, the C@BNNT$_{60}$ (with outer BNNT of 1.37 nm wall thickness) arrays showed significant enhancement in their shape recoverability, cyclic compressive properties (nearly full recovery after 1 compression cycle at a 50% strain, and ~76% recovery retained after 10 cycles) and energy dissipating properties (~60% E_d/E_a remained at a 50% strain after 100 cycles), as well as thermal stability in air owing to the improved mechanical and physicochemical properties of individual nanotubes due to the synergistic effect between the inner CNT and outer BNNT. The collective mechanical/thermal behaviour of the C@BNNT arrays would enable many potential applications such as energy dissipative devices and compressive thermal/mechanical contacts in harsh environments. This work also provides a new route to tune the mechanical properties of arbitrary CNT arrays by encapsulating with protective layers.

Acknowledgements

The authors would like to acknowledge support from the Institute for Sports Research (ISR), the NTU-A*STAR Silicon Technologies Centre of Excellence under the program grant no. 1123510003, and the Singapore Ministry of Education Academic Research Fund Tier 2 no. MOE2013-T2-2-050.

Notes and references

1 P. R. Bandaru, *J. Nanosci. Nanotechnol.*, 2007, **7**, 1239–1267.
2 S. Berber, Y.-K. Kwon and D. Tománek, *Phys. Rev. Lett.*, 2000, **84**, 4613.
3 B. Demczyk, Y. Wang, J. Cumings, M. Hetman, W. Han, A. Zettl and R. Ritchie, *Mater. Sci. Eng., A*, 2002, **334**, 173–178.
4 L. Vaccarini, C. Goze, L. Henrard, E. Hernandez, P. Bernier and A. Rubio, *Carbon*, 2000, **38**, 1681–1690.
5 J.-P. Salvetat, J.-M. Bonard, N. Thomson, A. Kulik, L. Forro, W. Benoit and L. Zuppiroli, *Appl. Phys. A*, 1999, **69**, 255–260.
6 S. B. Hutchens and S. Pathak, *Encyclopedia of Nanotechnology*, Springer, Netherland, 2012.
7 A. Cao, P. L. Dickrell, W. G. Sawyer, M. N. Ghasemi-Nejhad and P. M. Ajayan, *Science*, 2005, **310**, 1307–1310.
8 S. Pathak, Z. G. Cambaz, S. R. Kalidindi, J. G. Swadener and Y. Gogotsi, *Carbon*, 2009, **47**, 1969–1976.
9 C. Cao, A. Reiner, C. Chung, S.-H. Chang, I. Kao, R. V. Kukta and C. S. Korach, *Carbon*, 2011, **49**, 3190–3199.
10 J. Xu and T. S. Fisher, *IEEE Trans. Adv. Packag.*, 2006, **29**, 261–267.
11 J. Cho, C. Richards, D. Bahr, J. Jiao and R. Richards, *J. Micromech. Microeng.*, 2008, **18**, 105012.
12 C. Daraio, V. F. Nesterenko and S. Jin, *Appl. Phys. Lett.*, 2004, **85**, 5724–5726.
13 C. Daraio, V. F. Nesterenko, S. Jin, W. Wang and A. M. Rao, *J. Appl. Phys.*, 2006, **100**, 064309.
14 M. E. Kozlov, C. S. Haines, J. Oh, M. D. Lima and S. Fang, *J. Appl. Phys.*, 2009, **106**, 124311.
15 E. H. Teo, W. K. Yung, D. H. Chua and B. Tay, *Adv. Mater.*, 2007, **19**, 2941–2945.
16 P. D. Bradford, X. Wang, H. Zhao and Y. Zhu, *Carbon*, 2011, **49**, 2834–2841.
17 P.-C. Tsai and Y.-R. Jeng, *Carbon*, 2015, **86**, 163–173.
18 J. Suhr, P. Victor, L. Ci, S. Sreekala, X. Zhang, O. Nalamasu and P. Ajayan, *Nat. Nanotechnol.*, 2007, **2**, 417–421.
19 J. Suhr, N. Koratkar, P. Keblinski and P. Ajayan, *Nat. Mater.*, 2005, **4**, 134–137.
20 L. Ci, J. Suhr, V. Pushparaj, X. Zhang and P. Ajayan, *Nano Lett.*, 2008, **8**, 2762–2766.
21 S. B. Hutchens, L. J. Hall and J. R. Greer, *Adv. Funct. Mater.*, 2010, **20**, 2338–2346.
22 Y. Li, H.-i. Kim, B. Wei, J. Kang, J.-b. Choi, J.-D. Nam and J. Suhr, *Nanoscale*, 2015, **7**, 14299–14304.
23 O. Yaglioglu, A. Cao, A. J. Hart, R. Martens and A. Slocum, *Adv. Funct. Mater.*, 2012, **22**, 5028–5037.
24 A. Zbib, S. D. Mesarovic, E. Lilleodden, D. McClain, J. Jiao and D. Bahr, *Nanotechnology*, 2008, **19**, 175704.
25 Q. Zhang, Y. Lu, F. Du, L. Dai, J. Baur and D. Foster, *J. Phys. D: Appl. Phys.*, 2010, **43**, 315401.
26 S. Pathak, J. R. Raney and C. Daraio, *Carbon*, 2013, **63**, 303–316.
27 Y. Chen, J. Zou, S. J. Campbell and G. Le Caer, *Appl. Phys. Lett.*, 2004, **84**, 2430–2432.
28 S. Tsang, P. Harris and M. Green, *Nature*, 1993, **362**, 520–520.
29 P. Ajayan, T. Ebbesen, T. Ichihashi, S. Iijima, K. Tanigaki and H. Hiura, *Nature*, 1993, **362**, 522–525.
30 M. Xu, D. N. Futaba, T. Yamada, M. Yumura and K. Hata, *Science*, 2010, **330**, 1364–1368.
31 A. Kumar, M. R. Maschmann, S. L. Hodson, J. Baur and T. S. Fisher, *Carbon*, 2015, **84**, 236–245.
32 A. Misra, J. Raney, A. Craig and C. Daraio, *Nanotechnology*, 2011, **22**, 425705.
33 J. R. Raney, H.-L. Zhang, D. E. Morse and C. Daraio, *Carbon*, 2012, **50**, 4432–4440.
34 A. Rubio, J. L. Corkill and M. L. Cohen, *Phys. Rev. B: Condens. Matter*, 1994, **49**, 5081.
35 D. Golberg, Y. Bando, C. Tang and C. Zhi, *Adv. Mater.*, 2007, **19**, 2413–2432.
36 D. Golberg, Y. Bando, Y. Huang, T. Terao, M. Mitome, C. Tang and C. Zhi, *ACS Nano*, 2010, **4**, 2979–2993.
37 A. Shokuhfar, S. Ebrahimi-Nejad, A. Hosseini-Sadegh and A. Zare-Shahabadi, *Phys. Status Solidi A*, 2012, **209**, 1266–1273.

38 M. Santosh, P. K. Maiti and A. Sood, *J. Nanosci. Nanotechnol.*, 2009, **9**, 5425–5430.
39 N. G. Chopra and A. Zettl, *Solid State Commun.*, 1998, **105**, 297–300.
40 J. Wang, V. K. Kayastha, Y. K. Yap, Z. Fan, J. G. Lu, Z. Pan, I. N. Ivanov, A. A. Puretzky and D. B. Geohegan, *Nano Lett.*, 2005, **5**, 2528–2532.
41 P. Ahmad, M. U. Khandaker and Y. M. Amin, *Mater. Manuf. Processes*, 2015, **30**, 706–710.
42 X. Wang, Q. Wu, Z. Hu and Y. Chen, *Electrochim. Acta*, 2007, **52**, 2841–2844.
43 C. H. Lee, M. Xie, V. Kayastha, J. Wang and Y. K. Yap, *Chem. Mater.*, 2010, **22**, 1782–1787.
44 J. Wang, C. H. Lee and Y. K. Yap, *Nanoscale*, 2010, **2**, 2028–2034.
45 L. Guo and R. Singh, *Nanotechnology*, 2008, **19**, 065601.
46 C.-Y. Su, Z.-Y. Juang, K.-F. Chen, B.-M. Cheng, F.-R. Chen, K.-C. Leou and C.-H. Tsai, *J. Phys. Chem. C*, 2009, **113**, 14681–14688.
47 I. Mohai, M. Mohai, I. Bertóti, Z. Sebestyén, P. Németh, I. Z. Babievskaya and J. Szépvölgyi, *Diamond Relat. Mater.*, 2011, **20**, 227–231.
48 M. Mohai, I. Mohai, Z. Sebestyén, A. Gergely, P. Németh and J. Szépvölgyi, *Surf. Interface Anal.*, 2010, **42**, 1148–1151.
49 X. Yang, Z. Li, F. He, M. Liu, B. Bai, W. Liu, X. Qiu, H. Zhou, C. Li and Q. Dai, *Small*, 2015, **11**, 3710–3716.
50 C. Su, Z. Juang, Y. Chen, K. Leou and C. Tsai, *Diamond Relat. Mater.*, 2007, **16**, 1393–1397.
51 Y. Morihisa, C. Kimura, M. Yukawa, H. Aoki, T. Kobayashi, S. Hayashi, S. Akita, Y. Nakayama and T. Sugino, *J. Vac. Sci. Technol., B: Microelectron. Nanometer Struct.*, 2008, **26**, 872–875.
52 Y. J. Jeong and M. F. Islam, *Nanoscale*, 2015, **7**, 12888–12894.
53 K. M. Liew and J. Yuan, *Nanotechnology*, 2011, **22**, 085701.
54 J. Yuan and K. M. Liew, *Carbon*, 2011, **49**, 677–683.
55 R. Y. Tay, H. Li, S. H. Tsang, L. Jing, D. Tan, M. Wei and E. H. T. Teo, *Chem. Mater.*, 2015, **27**, 7156–7163.
56 Y. Shi, C. Hamsen, X. Jia, K. K. Kim, A. Reina, M. Hofmann, A. L. Hsu, K. Zhang, H. Li and Z.-Y. Juang, *Nano Lett.*, 2010, **10**, 4134–4139.
57 M. Bennett and R. Ker, *J. Anat.*, 1990, **171**, 131.
58 M. Bedewy, E. R. Meshot, H. Guo, E. A. Verploegen, W. Lu and A. J. Hart, *J. Phys. Chem. C*, 2009, **113**, 20576–20582.
59 S. B. Hutchens, A. Needleman and J. R. Greer, *J. Mech. Phys. Solids*, 2011, **59**, 2227–2237.
60 X. Li, J. Yin, J. Zhou and W. Guo, *Nanotechnology*, 2014, **25**, 105701.
61 H.-C. Chiu, S. Dogan, M. Volkmann, C. Klinke and E. Riedo, *Nanotechnology*, 2012, **23**, 455706.
62 A. Fallah and Y. Nakayama, *Carbon*, 2012, **50**, 1879–1887.
63 T. Kuzumaki and Y. Mitsuda, *Jpn. J. Appl. Phys.*, 2006, **45**, 364.
64 H. F. Bettinger, T. Dumitrică, G. E. Scuseria and B. I. Yakobson, *Phys. Rev. B: Condens. Matter*, 2002, **65**, 041406.